Available online at www.sciencedirect.com
SCIENCE DIRECT®
Carbohydrate Research 339 (2004) 1961–1966
Carbohydrate RESEARCH

Molecular dynamics (MD) simulations for the prediction of chiral discrimination of *N*-acetylphenylalanine enantiomers by cyclomaltoheptaose (β-cyclodextrin, β-CD) based on the MM–PBSA (molecular mechanics–Poisson–Boltzmann surface area) approach

Youngjin Choi and Seunho Jung*

Department of Microbial Engineering and Bio/Molecular Informatics Center, Konkuk University, 1 Hwayang-dong, Gwangjin-gu, Seoul 143-701, South Korea

Received 27 February 2004; accepted 26 May 2004
Available online 3 July 2004

Abstract—Molecular dynamics (MD) simulations were performed for the prediction of chiral discrimination of *N*-acetylphenylalanine enantiomers by cyclomaltoheptaose (β-cyclodextrin, β-CD). Binding free energies and various conformational properties were obtained using by the MM–PBSA (molecular mechanics Poisson–Boltzmann/surface area) approach. The calculated relative difference ($\Delta\Delta G_{binding}$) of binding free energy was in fine agreement with the experimentally determined value. The difference of rotameric distributions of guest *N*-acetylphenylalanine enantiomers complexed with the host, β-CD, was observed after the conformational analyses, suggesting that the conformational changes of guest captured within host cavity would be a decisive factor for enantiodifferentiation at a molecular level.

Keywords: Molecular dynamics simulations; Cyclodextrin; Chiral discrimination; Molecular mechanics

1. Introduction

Cyclomaltooligosaccharides (cyclodextrins, CDs) are cyclic oligosaccharides, which are composed of several α-D-glucose with (1→4) glycosidic linkages. Depending on the number of glucose residues, several CDs (six for α-, seven for β-, eight for γ-), and their derivatives have been utilized and developed for various biotechnological applications.[1] CDs have received much attention because of their ability to form inclusion complexes with a wide range of organic molecules.[2,3] As host molecules for the guest chemicals, CDs are able to make inclusion complexes with their unique hydrophobic cavities. These capabilities have been applied to various research fields such as solubility enhancement, drug delivery, chemical protection, separation technology, and supramolecular chemistry.[4,5] Particularly, enantiodifferentiation of optically active guests by CDs is one of the most important applications.[6,7] High-performance liquid chromatographic (HPLC) or capillary electrophoresis techniques using CDs as stationary or mobile phases have frequently been used for the enantioseparation of chiral chemicals.[8] NMR and X-ray crystallographic methods are useful for the investigation of molecular mechanisms for this kind of chiral recognition,[9] but these approaches to understand the detailed enantiodiscriminative mechanisms are resource intensive and time consuming.

In contrast to experimental methods, computational calculations could be advantageous for the analyses of

* Corresponding author. Tel.: +82-2-450-3520; fax: +82-2-452-3611; e-mail: shjung@konkuk.ac.kr

0008-6215/$ - see front matter © 2004 Elsevier Ltd. All rights reserved.
doi:10.1016/j.carres.2004.05.026

molecular mechanisms as well as effective conformational searching because these approaches could reproduce various ensembles for the enantioselective conformations induced by the inclusion complexation.[10] However, in the chiral recognition process, the guest molecules being discriminated have the same size, same shape, same molecular electrostatics, etc.; they can only be discerned when giving rise to slightly different diastereomeric responses once they associate with another chiral object or environment.[11] The intermolecular forces responsible for enantiodifferentiation are the same as those in other cases of molecular recognition, but the differences in corresponding binding free energies are usually much smaller in magnitude. That is the reason for the difficulty of enantioselective prediction in comparison with typical computational approaches.[12] Herein, we tried to apply the MM–PBSA (molecular mechanics Poisson–Boltzmann/surface area) method to investigate the chiral recognition between guest enantiomer and host cyclodextrin at the molecular level. The algorithm of this method combines explicit solvent molecular dynamics (MD) simulations with implicit solvation models, Poisson–Boltzmann analysis, and nonpolar solvation free-energy calculations to estimate binding free energies.[13] MD simulations are generally performed with periodic boxes of water molecules and a Particle Mesh Ewald (PME) method to calculate long-range electrostatics.[14] P. A. Kollman and co-workers have successfully calculated binding free energies for several biochemical systems using the MM–PBSA approach with just several hundred picosecond MD simulations and small trajectories.[14–18] The binding free energies are then obtained using an ensemble average of trajectories extracted from these MD simulations. In this study, β-cyclodextrin (β-CD) was used as the host and *N*-acetyl-D,L-phenylalanine (*N*-Ac-D-Phe or *N*-Ac-L-Phe) as the guest (Fig. 1), where these molecules were experimentally well-validated candidates for explanation of the molecular discrimination.[19–24] MD simulations for chiral discrimination were performed using the CHARMM program,[25] through which the difference of binding free energies between β-CD and *N*-Ac-Phe enantiomers was shown to be finely correlated with the published experimental result.[21]

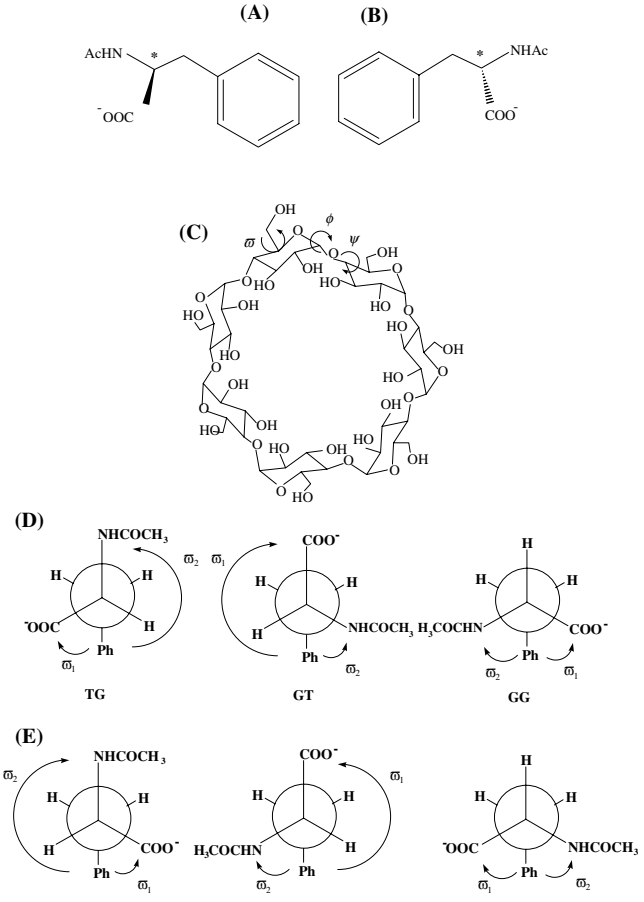

Figure 1. Schematic representation of the *N*-acetylphenylalanine and β-CD used in the MD simulations. (A) *N*-acetyl-D-phenylalanine (*N*-Ac-D-Phe), (B) *N*-acetyl-L-phenylalanine (*N*-Ac-L-Phe), (C) β-CD, (D) three rotamers for the *N*-Ac-D-Phe, and (E) three rotamers for the *N*-Ac-L-Phe; The chiral carbons of *N*-Ac-Phe enantiomers are indicated by asterisks. The torsion angles ϕ, ψ, and ϖ are defined as $\phi = \theta$(H1–C1–O1–C′4), $\psi = \theta$(C1–O1–C′4-H′4), and $\varpi = \theta$(O5–C5–C6–O6).

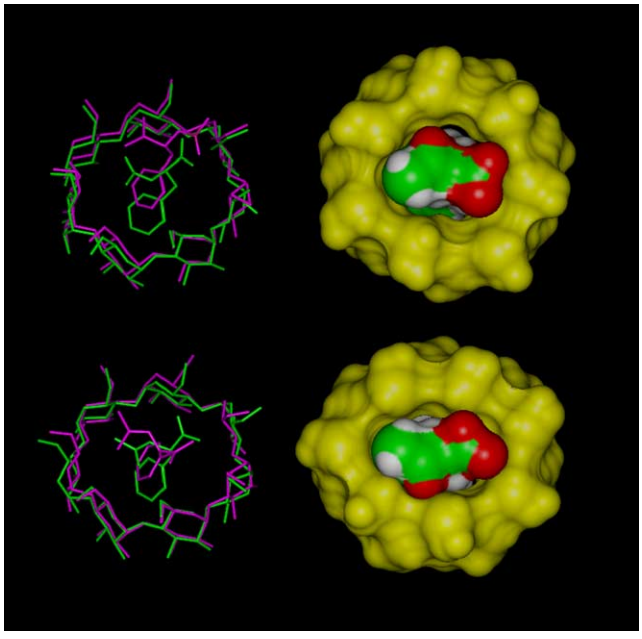

Figure 2. Superimposed snapshots (left) of *N*-Ac-Phe–β-CD complexes and their solvent-accessible surface area (right). Starting crystal geometries[22] (pink) and MD-generated aqueous conformations with the lowest binding energies (green) of the inclusion complexes for both enantiomers of *N*-Ac-Phe–β-CD complexes were shown, respectively. Relative orientations of the guest enantiomers in the β-CD cavities were maintained during the MD simulations. (top) *N*-Ac-D-Phe–β-CD and (bottom) *N*-Ac-L-Phe–β-CD complexes. Molecular surface rendering was performed with MD-generated conformations using the InsightII program.

2. Results and discussion

Figure 2 represents the superimposed X-ray crystal and MD-generated conformations[22] for each enantiomeric complex. The solvent-accessible surface area of each enantiomeric complex was generated from the MD simulations. The hydrophobic phenyl ring moiety of each *N*-Ac-Phe enantiomer was inserted to the cavity of β-CD while its carboxylate anion group was oriented to the narrow rim of the β-CD in each case. During the MD simulations, the phenyl ring of *N*-Ac-Phe for each complex was included by β-CD. Each glucopyranose ring of the β-CD has the primary hydroxyl dihedral angle (ω) close to −60° in accordance with the *gauche* effect.[26] Crystallographic structures were further refined using MD simulations in order to obtain the stable conformations in an equilibrium phase. The MM–PBSA method was applied to analyze the 2000 snapshots from the 1-ns MD simulations of the solvated *N*-Ac-D-Phe–β-CD complex and *N*-Ac-L-Phe–β-CD complex. Table 1 lists the components of molecular mechanics and solvation energies based on the MM–PBSA method. The calculation results for binding free energies showed an enantiodifferentiation between two inclusion complexes. The *N*-Ac-L-Phe–β-CD complex showed slightly stronger binding affinity compared with the *N*-Ac-D-Phe–β-CD complex. Average enantiodifference in the calculated binding free energy between each enantiomeric *N*-Ac-Phe and β-CD was −0.381 kJ/mol in comparison with the difference of experimental binding free energy of −0.260 kJ/mol,[21] where the entropy change of each enantiomeric complex upon binding is assumed to be equal.[14]

As shown in Table 1, the intermolecular vdW interaction (ΔE_{vdW}) and the nonpolar contribution to solvation ($\Delta E_{nonpolar}$) provide the driving force for binding. The favorable (negative) intermolecular electrostatic interaction is counteracted by the unfavorable (positive) electrostatic desolvation free energy (ΔE_{PB}). As a result, total electrostatic contribution ($\Delta E_{PB+elec}$) is unfavorable for binding. However, in the chiral recognition process, the critical component for enantiodiscrimination between two enantiomeric complexes was the relative difference of total electrostatic contribution ($\Delta\Delta E_{PB+elec} \approx -1.390$ kJ/mol), neither that of vdW interaction ($\Delta\Delta E_{vdW} \approx +0.921$ kJ/mol) nor that of nonpolar contribution to solvation ($\Delta\Delta E_{nonpolar} \approx +0.025$ kJ/mol) as shown in Table 1. Therefore, the difference of total electrostatic contribution ($\Delta\Delta E_{PB+elec}$) between guest and host would be a decisive factor that discriminates the relative binding affinity of these enantiomers to β-CD. To gain further insight into the chiral recognition between the β-CD and *N*-Ac-Phe enantiomers, we performed the analyses for the conformational features of the complexes. All the glycosidic dihedral angles (ϕ, ψ) of β-CD were populated around the region close to 0° (Fig. 3A and B). No enantiodifference in glycosidic dihedral angles of the host β-CDs complexed with the D- or L-enantiomer of *N*-Ac-Phe was observed. Neither were there any dihedral angles (ω) of glucopyranose ring(s) in the β-CD distinguished for the primary hydroxyl groups (Fig. 3C). These results indicate that conformational flexibility of the host β-CD does not act as a major driving force for the enantiodifferentiation. However, the rotameric distributions of guest *N*-Ac-Phe enantiomers showed conformational changes upon complexation with β-CD. Figure 4 shows a dihedral angle map of *N*-Ac-Phe enantiomers complexed with the β-CD, where each rotameric notation is depicted in Figure 1. A major portion of both *N*-Ac-Phe enantiomers was obtained as *gt* rotamers and a minor portion was observed as *tg* rotamers. No *gg* rotamers were observed. Based on this conformational analysis, the *tg* to *gt* ratio for *N*-Ac-D-Phe rotamers was to be 0.027 (2.6:97.4), and the ratio for *N*-Ac-L-Phe was obtained as 0.043 (4.1:95.9). A relative change of the *tg*

Table 1. Relative difference of binding (free) energy (kJ/mol, $\Delta\Delta G_{binding}$) resulting from molecular mechanics/Poisson–Boltzmann surface area analysis for the *N*-Ac-D-Phe–β-CD and the *N*-Ac-L-Phe–β-CD complexes

	N-Ac-D-Phe–β-CD	N-Ac-L-Phe–β-CD	$\Delta\Delta E(G)_{L-D}$
ΔE_{vdW}	−71.949	−71.028	+0.921
ΔE_{elec}	−135.212	−137.862	−2.650
ΔE_{gas}	−207.161	−208.890	−1.729
$\Delta E_{nonpolar}$	−7.300	−7.275	+0.251
ΔE_{PB}	183.163	185.519	+1.260
$\Delta E_{solvation}$	175.862	177.147	+1.285
$\Delta E_{PB+elec}$	47.951	46.561	−1.390
$\Delta E_{total,PB}$	−31.299	−31.680	−0.381
$\Delta G_{binding}$	−31.299−($T\Delta S$)[a]	−31.680−($T\Delta S$)[a]	−0.381[b] (−0.260)[c]

The components of the total binding energy are also shown (kJ/mol): van der Waals (ΔE_{vdW}), electrostatic (ΔE_{elec}), gas ($\Delta E_{gas} = \Delta E_{vdW} + \Delta E_{elec}$), nonpolar solvation ($\Delta E_{nonpolar}$), polar solvation ($\Delta E_{PB}$), solvation ($\Delta E_{solvation} = \Delta E_{nonpolar} + \Delta E_{PB}$), total electrostatic contribution ($\Delta E_{PB+elec}$), binding energy ($\Delta E_{total,PB}$).

[a] The entropy change between two enantiomers upon binding is assumed to be equal[14] ($\Delta S_L \approx \Delta S_D$).

[b] $\Delta\Delta G_{binding} = \Delta G_{binding}$ (*N*-Ac-L-Phe–β-CD)−$\Delta G_{binding}$ (*N*-Ac-D-Phe–β-CD).

[c] The data in parentheses is the experimentally determined value for binding free energy.[21]

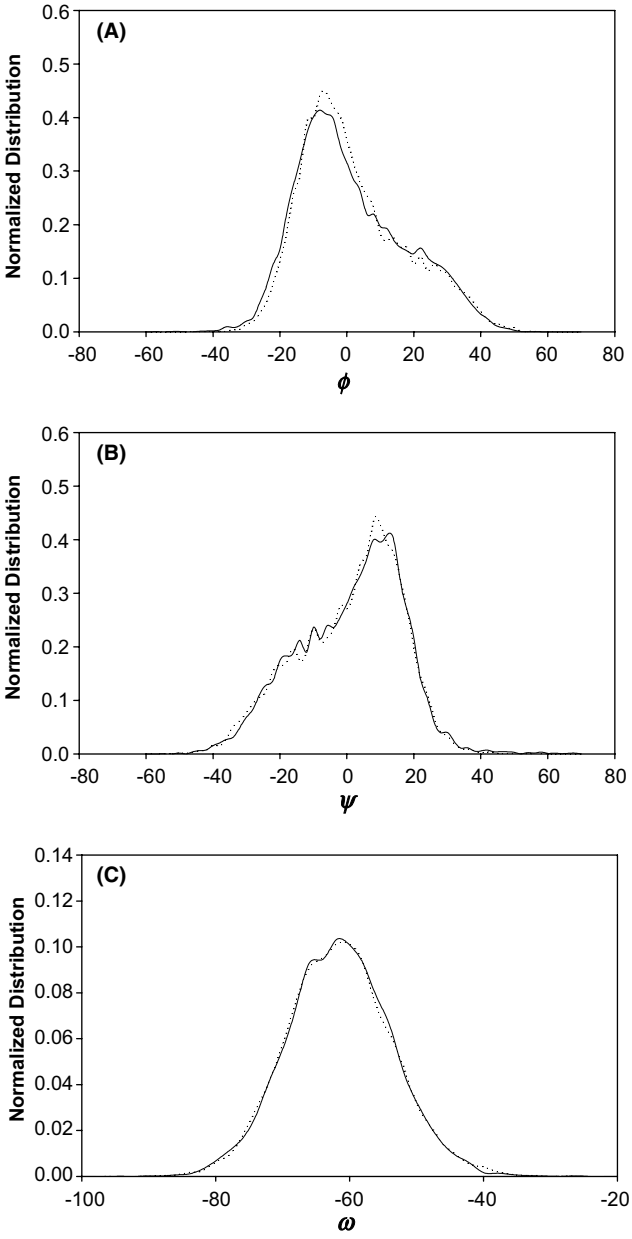

Figure 3. Populations of the glycosidic dihedral angles and the primary alcohol dihedral angles for the β-CD. (A) glycosidic ϕ angle (B) glycosidic ψ angle (C) primary alcohol dihedral angle ω, respectively. Solid lines denote *N*-Ac-L-Phe–β-CD complex and dashed lines indicate *N*-Ac-D-Phe–β-CD complex.

the rotameric state was observed for the enantiodifferentiation process. The carboxylate anion groups of *tg* rotamers have more stable and closer contact, through the electrostatic interactions, with the hydroxyl groups of β-CD compared with *gt* rotamers based on the energy-minimized structures of rotamers captured by β-CD. In case of the L-enantiomeric complex, the intermolecular electrostatic energy for the energy-minimized *gt* rotameric complex was −113.315 kJ/mol and that of the *tg* rotameric complex was −137.008 kJ/mol. The intermolecular vdW energies were not distinguished

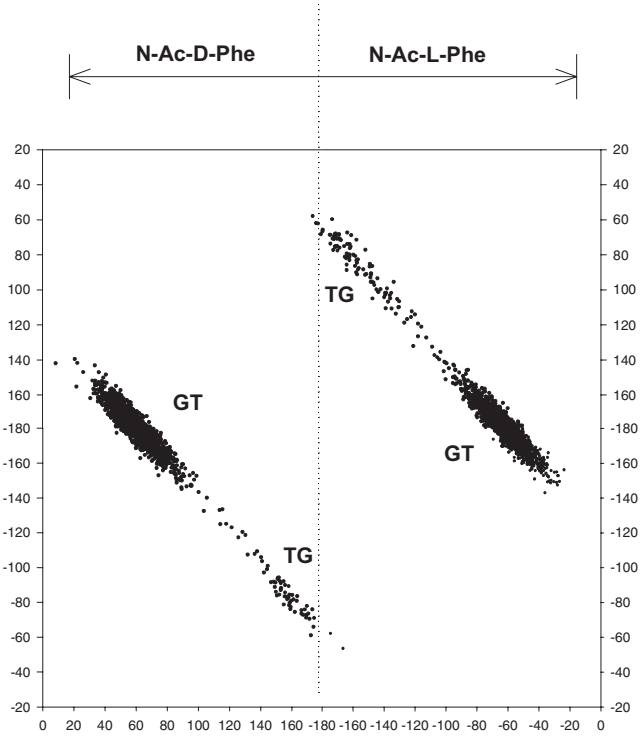

Figure 4. Scatter plots for the dihedral angle distributions of *N*-Ac-Phe enantiomers within a β-CD cavity during the MD simulations. Both enantiomers present as a *gt* or *tg* rotameric conformation.

between both rotameric complexes ($\Delta E_{\mathrm{vdW\_gt\,complex}} = -83.176$ kJ/mol, $\Delta E_{\mathrm{vdW\_gt\,complex}} = -82.590$ kJ/mol). Since the molecular recognition processes by host–guest complexations are wholly dependent on the noncovalent interactions, the relative difference of rotamer ratio (gt/tg) of the guest molecules inside the CD cavity might be an index for the effective chiral discrimination. This fact indicated that the chiral discrimination processes would be determined mainly by the conformational changes of the chiral guest molecule complexed within β-CD.[27]

In conclusion, our results indicate that rotamer population changes of *N*-Ac-Phe enantiomers, not the β-CD, made a critical contribution to the chiral discrimination in this case. The slightly stronger electrostatic interaction in the L-enantiomer complex, as a consequence of difference of guest rotameric distribution, could explain the difference of binding free energy observed in the complexation of *N*-Ac-Phe enantiomers with β-CD. A fine agreement was obtained for the difference of experimental binding free energy ($\Delta\Delta G_{\mathrm{binding}}$) to *N*-Ac-Phe enantiomers with β-CD, suggesting that the conformational changes of *N*-Ac-Phe enantiomers captured within β-CD would be a decisive factor for enantiodifferentiation at a molecular level. We are not sure, at present, of the generality that the rotamer population changes of guest molecules captured by host induce different chiral interactions. However, comparing with the degree of motional and structural

flexibilities between guest and host, guest flexibility within the host cavity would make, in general, a major contribution to the chiral discrimination. Further research into the generality of this phenomenon will be undertaken.

3. Experimental

3.1. Construction of the molecular models and protocol of molecular dynamics simulations

The starting configurations of the simulations were representative X-ray crystal structures of *N*-Ac-Phe enantiomers bound to the β-CD.[22] The following missing hydrogen atoms in the X-ray coordinates were built with InsightII/Builder program (version 2000, Accelrys Inc., San Diego, USA). The geometry of these molecular models was fully optimized before the MD runs. Their molecular structures are shown in Figure 1. A Na^+ ion was added to neutralize each system. TIP3P three-site rigid water model[28] was used to solvate the *N*-Ac-Phe enantiomer–β-CD complexes and counterions. Water molecules were removed if they were closer than 2.6 Å to any heavy atoms of the complex. In summary, each system was constructed using periodic boundary conditions with a cubic box of dimension $30\times30\times30$ Å, consisting of a 1:1 *N*-Ac-Phe enantiomer–β-CD complex, a counterion, and 930 TIP3P water molecules. The system was minimized by 1000 steps of conjugate gradient, followed by the adopted basis Newton–Raphson protocol until the root-mean-square gradient was less than 0.004 kJ/mol. The MD simulations were performed using the CHARMM 28b2 program with parm22 all-atom force field in the isothermal–isobaric ensemble ($P = 1$ bar, $T = 298$ K). The parameter values for the β-CD were modified according to the sugar22 parameter set of the CHARMM. The particle mesh Ewald summation method[29] was used to treat the long-range electrostatic interactions. The bond lengths of water molecules were constrained with the SHAKE algorithm.[30] The time step was 1.0 fs, and the nonbonded pair list was updated every 50 steps. The short-range nonbonded interactions were truncated with a 13-Å cutoff. The temperature and pressure of the system was regulated using the Langevin piston method in conjunction with Hoover's thermostat.[31] The system was gradually heated to 298 K and maintained for 100 ps as an equilibrium phase. The production MD trajectory with one snapshot per 0.5 ps was collected for 1000 ps.

3.2. Binding free-energy calculation methods

The MM–PBSA methodology was applied to estimate the free energies of binding from the absolute energies in the gas phase (E_{MM}), and solvation free energies ($G_{PB} + G_{nonpolar}$) for each guest, host, and complex.[13] The difference of binding free energy between the *N*-Ac-D-Phe and *N*-Ac-L-Phe complexes is defined as:

$$\Delta\Delta G_{binding} = \Delta G_{binding\_L\ enantiomer} - \Delta G_{binding\_D\ enantiomer} \quad (1)$$

$$\Delta G_{binding} = \Delta G_{(complex)} - [\Delta G_{(host)} + \Delta G_{(guest)}] \quad (2)$$

$$G_{molecule} = \langle E_{MM}\rangle + \langle G_{PB}\rangle + \langle G_{nonpolar}\rangle - TS \quad (3)$$

$$E_{MM} = E_{vdw} + E_{elec} \quad (4)$$

where $\langle\ \rangle$ denotes an average over a set of snapshots along an MD trajectory. E_{vdw} and E_{elec} denote vdW and electrostatic energies, respectively. For the analysis of $\Delta G_{binding}$ both the water molecules and counterions were then deleted. The polar contribution to the solvation free energy (G_{PB}) was calculated by solving the Poisson–Boltzmann equation with the PBEQ module of the CHARMM program. The polar solvation process is equivalent to the transfer of a molecule from one medium with dielectric constant equal to that of the interior of the molecule to another medium with dielectric constant equal to that of the exterior of the molecule. For the PBEQ calculation, the grid spacing was set to 0.5 Å, the molecule was filled with the grid box, 2000 iterations were performed to ensure the maximum change in potential was less than $2\times10^{-6}\,kT/e$, and the dielectric constant inside and outside the molecule was 1.0 and 80.0, respectively. The nonpolar solvation contribution includes cavity creation in water and vdW interactions between the modeled nonpolar molecule and water molecules. This term can be imagined as transferring a nonpolar molecule with the shape of the host or guest from vacuum to water. This transfer free energy is described as:[32]

$$\Delta G_{nonpolar} = \gamma A + b$$

where A is the solvent-accessible surface area calculated by the CHARMM program, and γ and b are 0.02269 kcal/mol Å^2 and 3.851 kJ/mol,[26] respectively, which were derived from experimental transfer energies of hydrocarbons. The probe radius was 1.4 Å.

In Eq. (3), S is the entropy changes for the host–guest complexation. The solvent entropy changes caused by polarization and cavity formation are included in the polar and nonpolar solvation-free energy terms. The solute entropy changes are almost similar because the structural properties are identical to each other in enantiomers. Thus, in this study the entropy change of each enantiomeric complex upon binding is assumed to be equal.[14,33]

Acknowledgements

This study was supported by a grant of the Korea Health 21 R&D Project, Ministry of Health and Welfare, Republic of Korea (02-PJ1-PG3-51103-0001), SDG.

References

1. D'Souza, V. T.; Lipkowitz, K. B. *Chem. Rev.* **1998**, *98*, 1741–2076.
2. Singh, M.; Sharma, R.; Banerjee, U. C. *Biotechnol. Adv.* **2002**, *20*, 341–359.
3. Kim, H.; Jeong, K.; Lee, S.; Jung, S. *J. Comput. Aided Mol. Des.* **2002**, *16*, 601–610.
4. Stella, V. J.; Rao, V. M.; Zannou, E. A.; Zia, V. *Adv. Drug Delivery Rev.* **1999**, *36*, 3–16.
5. Schneiderman, E.; Stalcup, A. M. *J. Chromatogr. B.* **2000**, *745*, 83–102.
6. Armstrong, D. W.; Ward, T. J.; Armstrong, R. D.; Beesley, T. E. *Science* **1986**, *232*, 1132–1135.
7. Cram, D. J. *Science* **1988**, *240*, 760–767.
8. Lipkowitz, K. B. *Chem. Rev.* **1998**, *98*, 1829–1873.
9. Lee, S.; Jung, S. *Carbohydr. Res.* **2003**, *338*, 1143–1146.
10. Maier, N. M.; Schefzick, S.; Lombardo, G. M.; Feliz, M.; Rissanen, K.; Lindner, W.; Lipkowitz, K. B. *J. Am. Chem. Soc.* **2002**, *124*, 8611–8629.
11. Lipkowitz, K. B.; Coner, R.; Peterson, M. A. *J. Am. Chem. Soc.* **1997**, *119*, 11269–11276.
12. Dodziuk, H.; Lukin, O. *Chem. Phys. Lett.* **2000**, *327*, 18–22.
13. Srinivasan, J.; Cheatham, T. E.; Cieplak, P.; Kollman, P. A.; Case, D. A. *J. Am. Chem. Soc.* **1998**, *120*, 9401–9409.
14. Huo, S.; Massova, I.; Kollman, P. A. *J. Comput. Chem.* **2002**, *23*, 15–27.
15. Bea, I.; Jaime, C.; Kollman, P. A. *Theor. Chem. Acc.* **2002**, *108*, 286–292.
16. Gouda, H.; Kuntz, I. D.; Case, D. A.; Kollman, P. A. *Biopolymers* **2003**, *68*, 16–34.
17. Wang, J.; Morin, P.; Wang, W.; Kollman, P. A. *J. Am. Chem. Soc.* **2001**, *123*, 5221–5230.
18. Kuhn, B.; Kollman, P. A. *J. Med. Chem.* **2000**, *43*, 3786–3791.
19. Clark, J. L.; Stezowski, J. J. *J. Am. Chem. Soc.* **2001**, *123*, 9880–9888.
20. Rekharsky, M. V.; Inoue, Y. *J. Am. Chem. Soc.* **2002**, *124*, 12361–12371.
21. Rekharsky, M. V.; Inoue, Y. *J. Am. Chem. Soc.* **2002**, *124*, 813–826.
22. Alexander, J. M.; Clark, J. L.; Brett, T. J.; Stezowski, J. J. *Proc. Natl. Acad. Sci. U.S.A.* **2002**, *99*, 5115–5120.
23. Inoue, Y. *Ann. Rep. NMR Spectrosc.* **1993**, *27*, 59–101.
24. Takahashi, S.; Suzuki, E.; Nagashima, N. *Bull. Chem. Soc. Jpn.* **1986**, *59*, 1129–1132.
25. Brooks, B. R.; Bruccoleri, R. E.; Olafson, B. D.; States, D. J.; Swaminathan, S.; Karplus, M. *J. Comput. Chem.* **1983**, *4*, 187–217.
26. Kirschner, K. N.; Woods, R. J. *Proc. Natl. Acad. Sci. U.S.A.* **2001**, *98*, 10541–10545.
27. Kano, K. *J. Phys. Org. Chem.* **1997**, *10*, 286–291.
28. Jorgensen, W. L. *J. Chem. Phys.* **1982**, *77*, 4156–4163.
29. Darden, T.; York, D.; Pedersen, L. *J. Chem. Phys.* **1993**, *98*, 10089–10092.
30. Ryckaert, J. P.; Ciccotti, G.; Berendsen, H. J. C. *J. Comput. Phys.* **1977**, *23*, 327–341.
31. Feller, S. E.; Zhang, Y.; Pastor, R. W.; Brooks, B. R. *J. Chem. Phys.* **1995**, *103*, 4613–4621.
32. Sitkoff, D.; Sharp, K. A.; Honig, B. *J. Phys. Chem.* **1994**, *98*, 1978–1988.
33. Wang, W.; Lim, W. A.; Jakalian, A.; Wang, J.; Wang, J.; Luo, R.; Bayly, C. I.; Kollman, P. A. *J. Am. Chem. Soc.* **2001**, *123*, 3986–3994.